Design of ultra-compact composite plasmonic Mach-Zehnder interferometer for chemical vapor sensing

Souvik Ghosh[a] and B.M.A. Rahman[a]

[a]Department of Electrical and Electronic Engineering, City, University of London, UK

ABSTRACT

Following the Industrial advancements in the last few decades, highly flammable chemicals, such as ethanol (CH_3CH_2OH) and methanol (CH_3OH) are widely being used in daily life. Ethanol have some degrees of carcinogenic effects in human whereas acute and chronic exposer of methanol results blurred vision and nausea. Therefore, accurate and efficient sensing of these two vapors in industrial environment are of high priorities. We have designed a novel, ultra-compact chemical vapor sensor based on composite plasmonic horizontal slot waveguide (CPHSW) where a low-index porous-ZnO (P-ZnO) layer is sandwiched in between top silver metal and lower silicon layers. Different P-ZnO templates, such as nano-spheres, nano-sheets and nanoplates could be used for high-selectivity of ethanol and methanol at different temperatures. The Lorentz-Lorenz model is used to determine the variation of P-ZnO refractive index (RI) with porosity and equivalent RI of P-ZnO layer for capillary condensation of different percentage of absorbed vapor. An in-house, new divergence modified finite element method is used to calculate effective index and attenuation sensitivity. Plasmonic modal analyses of dominant quasi-TM mode shows a high 42% power confinement in the slot. Next, an ultra-compact MZI incorporating a few micrometres long CPHSW is designed and analysed as a transducer device for accurate detection of effective index change. The device performance has been studied for different percentage of ethanol into P-ZnO with different porosity and a maximum phase sensitivity of >0.35 a.u. is achieved for both the chemical vapors at a mid-IR operating wavelength of 1550 nm.

Keywords: Composite plasmonic waveguide, plasmonic mode analysis, Mach-Zehnder interferometer (MZI), finite element method

1. INTRODUCTION

Photonic device integration and nano-dimension electronics are challenging due to ingrained diffraction limit of electromagnetic energy guided by dielectric media. This difficulty can be overcame by application of surface plasmon polaritons (SPPs). Surface plasmon (SP) is a surface wave which is a hybrid of electromagnetic wave and free electrons at the metal surface. Metal has negative dielectric constant whereas dielectrics show a positive value at the optical and near infra-red (IR) region. This complimentary material property at the metal-dielectric interface excites electromagnetic surface wave that propagates until the field dies by material absorptions and scattering into surrounding media. Comparing other nano-scale waveguides, such as, high-index contrast silicon-on-insulator (SOI) nano-wires and photonic crystals (PCs), surface plasmon (SP) shows a true sub-diffraction limited light confinement. The light guiding characteristics of conventional dielectric waveguides and a pure plasmonic waveguides[1] are opposite in nature. A high-index contrast dielectric waveguide confines light in the high index region results a very low propagation loss. Besides, a pure metal plasmonic waveguide provides a sub-wavelength scale light guiding but with a very high propagation loss.[1] Thus, a composite waveguide - a combination of metal and dielectric materials is very attractive to channelize the unique features of SPPs in the field of linear, non-linear photonic devices[2,3] and sensing applications.[4]

Our proposed composite plasmonic vapor sensor waveguide (CPWG) contains a horizontal layer of porous ZnO (P-ZnO) as a low index medium which is sandwiched in between high index silicon (Si) and lossy metal (Ag). Light guides through the low index P-ZnO layer where the chemical vapor get absorbed and condensed into

Further author information: (Send correspondence to Souvik Ghosh)
Souvik Ghosh: E-mail: souvik.ghosh.1@city.ac.uk, Telephone: +44 7405137454
B. M. A. Rahman.: E-mail: b.m.a.rahman@city.ac.uk

liquid due to capillary condensation. A cross-section of the CPWG is accurately designed and optimized by using our in-house newly modified full vectorial finite element method (FV-FEM). Finally, a compact Mach-Zehnder interferometer (MZI) is designed and its phase sensitivity is analyzed for ethanol vapor sensing.

2. MODIFIED FULL VECTORIAL FINITE ELEMENT METHOD (FV-FEM)

The formulation of electromagnetic (EM) field into variational form was first proposed by Berk in 1956.[5] Among several approaches (**E**-field, **E**+**H**-field and E_z+H_z-field), the **H**-field based formulation is more advantageous as the **H**-field is naturally continuous at the dielectric interfaces.[6] We modified our previously proposed penalty based approach[7] to eliminate the spurious solutions. In the penalty method, a global weighting factor of $1/n_{eff}^2$ was used in associate with the divergence equation ($div.\mathbf{B} = 0$). This is efficient for modal analysis of passive dielectric waveguides. However, this method is inadequate for plasmonic waveguide modal solutions. Thus, a more direct approach is proposed where, local material permittivities (positive and negative) are considered into additional divergence-divergence part. During global matrix formations, individual local dielectric constant of the discretized triangular element is considered. Thus, the modified form of the functional (J_e) with divergence-divergence inner product is

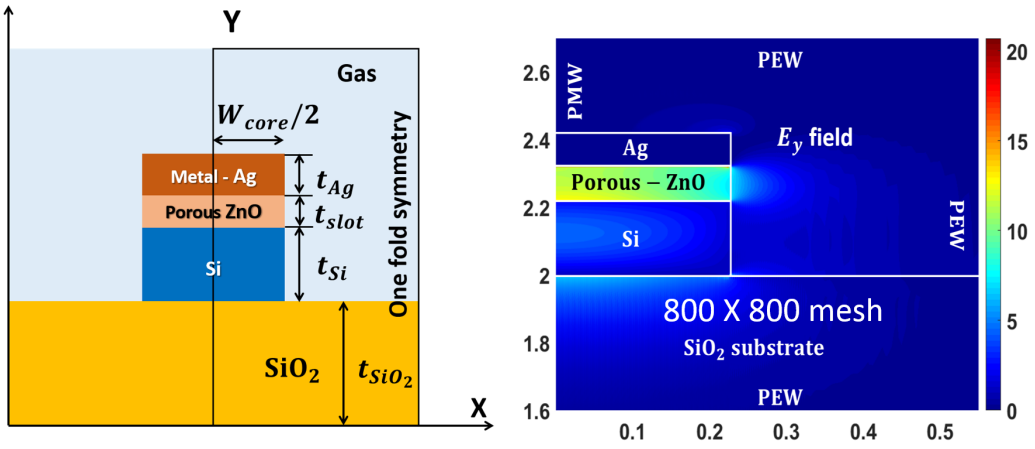

Figure 1. Schematic cross-section of horizontal slotted CPWG and its simulated electric field distributions by modified FV-FEM.

$$J_e = \langle \hat{\epsilon_r}^{-1} (\nabla \times \mathbf{H}), (\nabla \times \mathbf{H}) \rangle + \langle \hat{\epsilon_r}^{-1} (\nabla \cdot \mathbf{H}), (\nabla \cdot \mathbf{H}) \rangle - \omega^2 \langle \hat{\mu_r} \mathbf{H}, \mathbf{H} \rangle \tag{1}$$

Here the parameters ω, $\hat{\epsilon}$ and $\hat{\mu}$ are the angular frequency, permittivity and permeability tensors, respectively. ω^2 denotes the eigenvalue. The braces in 1 indicates the inner product, $\langle \mathbf{A}, \mathbf{B} \rangle = \iint \mathbf{B}^* \cdot \mathbf{A}\, dxdy$. Now, the Euler form of the 1 not only satisfy the Helmholtz's equation but also satisfy the Maxwell's two divergence equations. Here the J_e denotes the standard variational functional for a single triangular element. For 2D modal solutions, the time dependence $e^{-j\omega t}$ is assumed throughout and for a waveguide the z-dependency in the direction of propagation is taken as $e^{-j\omega z}$. Finally, using minimum theorem ($\delta J = 0$) we obtain a compact standard and stationary eigenvalue equation.

$$\omega^2 = \frac{\iint \left[(\nabla \times \mathbf{H})^* \cdot \hat{\epsilon_r}^{-1} (\nabla \times \mathbf{H}) + (\nabla \cdot \mathbf{H})^* \hat{\epsilon_r}^{-1} (\nabla \cdot \mathbf{H}) \right] dxdy}{\iint \mathbf{H}^* \hat{\mu_r} \cdot \mathbf{H}\, dxdy} \tag{2}$$

The solution of Eq. 2 provides the eigenvalues and associated eigenvectors. The modal propagation constant and effective indices ($N_{eff} = n_{eff} + jk_{eff}$) can be calculated from the eigenvalues whereas, the associated eigenvectors represent the modal field distributions. The propagation length (L_p) defines the waveguide length where modal power becomes $1/e$ times of its initial value and this can be given as, $L_p = \lambda/4\pi k_{eff}$. Additionally,

the modal attenuation (α) can be obtained as, $\alpha = 4.343/L_p$. CPWG design and optimization requires an accurate evaluation of slot confinement. As the E and H field profiles in a plasmonic mode have significantly different mode field profiles, we have followed the slot power confinement (Γ_{slot}) calculation that included the z-component of modal Poynting vector ($= \frac{1}{2}(\mathbf{E} \times \mathbf{H}^*) \cdot \hat{z}$), which considers the effect of both E and H fields:

$$\Gamma_{slot} = \frac{\iint_{slot} Re\,(\mathbf{E} \times \mathbf{H}^*) \cdot \hat{z}\; dxdy}{\iint_{total} Re\,(\mathbf{E} \times \mathbf{H}^*) \cdot \hat{z}\; dxdy} \tag{3}$$

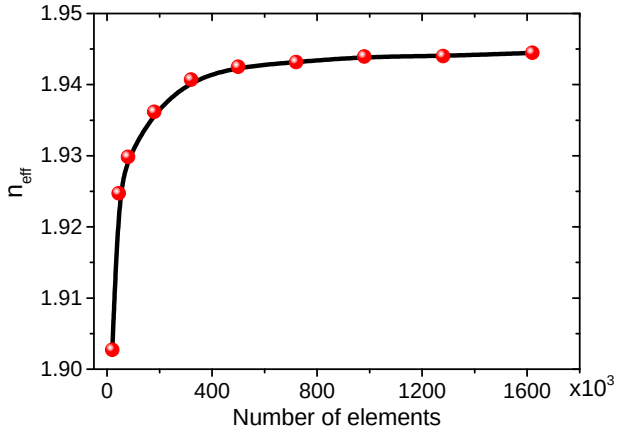

Figure 2. Variation of the effective index (n_{eff}) with different number of elements in the mesh.

During simulation, different mesh sizes have been used to obtain the convergence of the mode effective index. The effective index variation with the different mesh elements have been shown in Fig. 1. An acceptable result can be obtained by a lower 400×400 mesh (320,000 elements) distributions. Throughout the simulation process, we have considered 800×800 mesh for computation domain discretization.

3. POROUS ZNO CAPILLARY CONDENSATION

P-ZnO has lower refractive index than a bulk ZnO, as the material pores are filled with air (n = 1). The equivalent refractive index has an inverse relation with the number of pores per unit volume, called porosity (P). Increased curved empty area due to porosity results the absorption and condensation of vapor or gas substances. 2 to 50 nm mesoporous P-ZnO layer possess the surface area around 1000 m2/g. When the porous layer is kept in contact with the measuring vapor the air (n = 1) filled spaces are replaced by condensed liquid chemical (n ¿ 1). Depending on the different absorbed volume fraction and condensed liquid chemical, the effective refractive index as well as dielectric constant of P-ZnO changes. To make our device efficient, different P-ZnO layer templates, such as, porous flakes composed ZnO spheres [28], P-ZnO nanosheets [29] and nanoplates [30] could be used. P-ZnO spheres, nanosheets and nanoplates are mesoporous with pore diameters ranging from 2 to 50 nm. The P-ZnO sphere layer shows an enhanced selective response to 100 ppm ethanol at 280 C. Similarly, a strong response in ethanol sensing can be observed around 400 to 450 C for nanosheets and nanoplates [29], [30]. These P-ZnO configurations show excellent selectivity and much lower response and recovery time to ethanol and methanol vapor. Use of these P-ZnO templates make the CPWG more stable and efficient for ethanol and methanol vapor sensing.

Among various effective quantitative models, such as, Maxwell-Garnet theory, Bruggeman model and Lorentz-Lorenz model, in our work, we used the Lorentz-Lorenz model[8] to determine the effective refractive index of P-ZnO and equivalent refractive index (n_e). The variation of equivalent refractive index of P-ZnO layer with porosity (P) and ethanol volume fraction are shown in Fig. 3

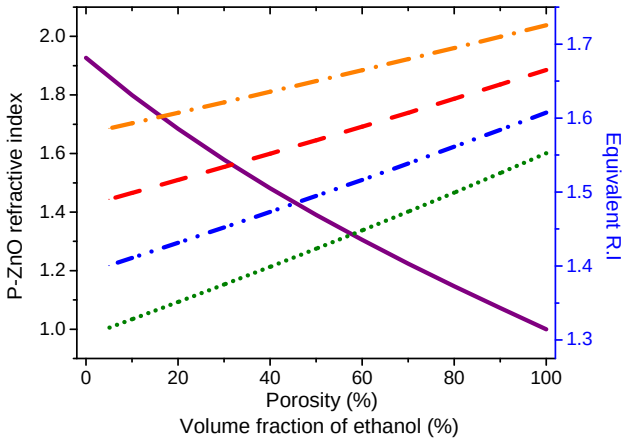

Figure 3. P-ZnO refractive index variation with porosity (P%) and change of equivalent refractive index of P-ZnO with volume fraction (V) of condensed liquid chemical. The orange, red, blue and purple lines represents the ZnO layer with porosity, P = 30%, 40%, 50% and 60%, respectively.

4. DESIGN AND OPTIMIZATION OF CPWG

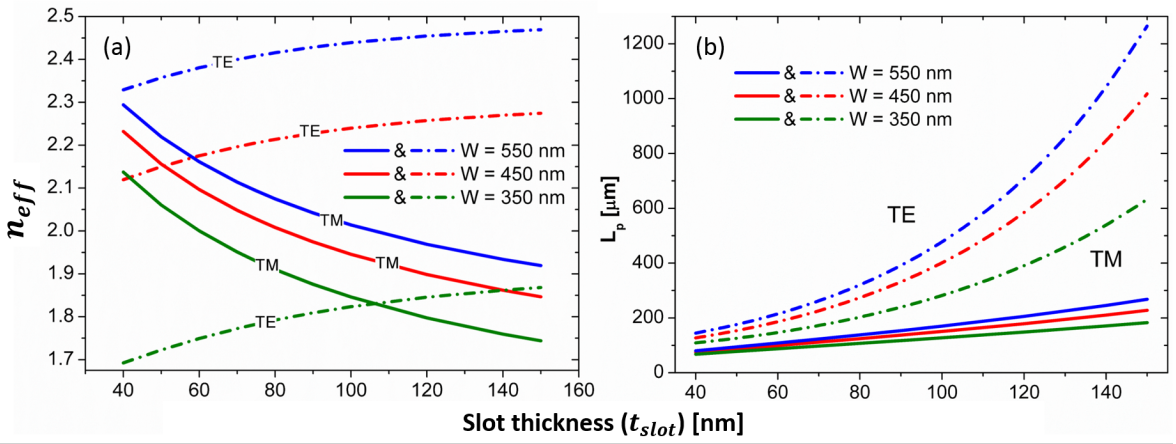

Figure 4. Real part of effective index (n_{eff}) and propagation length (L_p) variation with slot thickness (t_{slot}) of the CPWG. The solid and dashed-dotted lines indicate the variation of quasi-TM and TE modes, respectively. Three different core widths, W = 350, 450 and 550 nm and Si height, $t_Si = 220nm$ have been considered for simulations.

Figs. 4 (a) and (b) show the variation of the real part of the effective index, n_{eff} and modal propagation length L_p against the horizontal slot dimension t_{slot}, respectively. Three different widths (W) 350 nm, 450 nm and 550 nm are considered and shown by green, red and blue lines, respectively. Dashed-dotted and solid lines depict the variations of the quasi-TE and TM modes, respectively. As t_{slot} increases the n_{eff} decreases gradually for fundamental quasi-TM mode but increases for fundamental quasi-TE mode, respectively. Here for CPWG, the effective dominant mode for sensing is the quasi-TM supermode where a surface plasmonic mode is coupled with dielectric mode into low index slot region. The L_p variations with t_{slot} in Fig. 4(b) show a faster increment for quasi-TE as the light is guided by the low-loss dielectric regions but the quasi-TM mode shows a comparative slow increment with the P-ZnO dielectric layer thickness as the field profile is dominated by the SPPs generated by the lossy metal-dielectric interface.

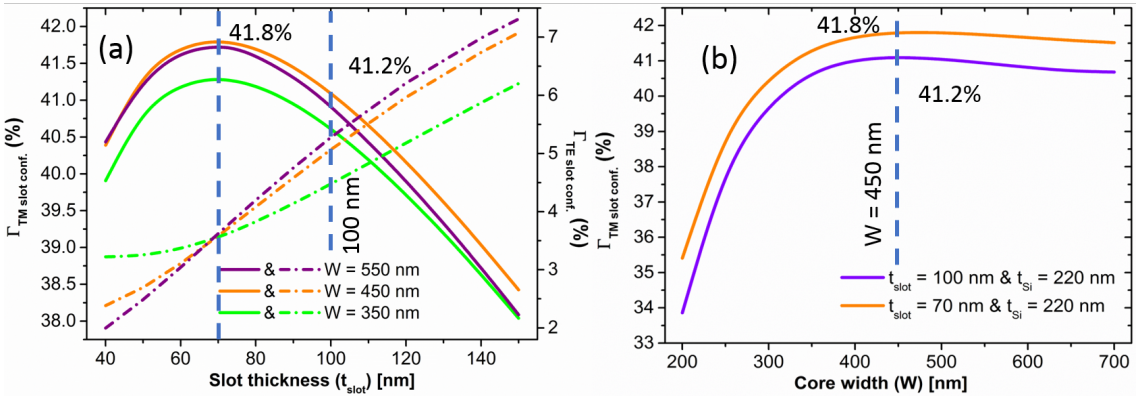

Figure 5. (a) shows the quasi-TM and TE slot confinement variation with t_{slot} for three different fixed core widths, W = 350, 450 and 550 nm. Solid and dashed-dotted lines depict the quasi-TM and TE modes, respectively. (b) shows the variation of the TM slot confinement with the CPWG core width for two fixed slot thicknesses, t_{slot} = 70 and 100 nm.

Figs. 5 (a) and (b) indicate the quasi-TE and TM slot confinements with the t_{slot} and W, respectively. For three fixed W, the $\Gamma_{TMslotconf.}$ increases, reaches a maximum value of 41.8% at t_{slot} = 70 nm and then decreases gradually with further increment. It can be noticed that the CPWG with W = 450 nm, shown by the orange solid line, confines higher electromagnetic energy than other two core widths (550 and 350 nm), shown by purple and green solid lines, respectively. The TE slot confinement also increases with the t_{slot}. However, it confines very low power compared to the quasi-TM modes. For a plasmonic waveguide sensor, the slot confinement due to SPP and dielectric supermode is our most concern. Thus, we focused only on $\Gamma_{TMslotconf.}$ and the maximum confinement is obtained for optimized slot thickness, t_{slot} = 70 nm. Further optimization of W for 70 nm and 100 nm slot thicknesses have been carried out in Fig. 5(b). With W, the $\Gamma_{TMslotconf.}$ increases and confines maximum 41.80% and 41.09% TM field into 70 and 100nm slot, respectively at W = 450 nm. It can be seen that the power confinement by the 70 and 100 nm slot have a negligible difference. Thus, the optimized CPWG designed parameters could be listed as, W = 450 nm, t_{slot} = 100 nm, t_{Si} = 220 nm and t_{Ag} = 100 nm for 40% ZnO porosity.

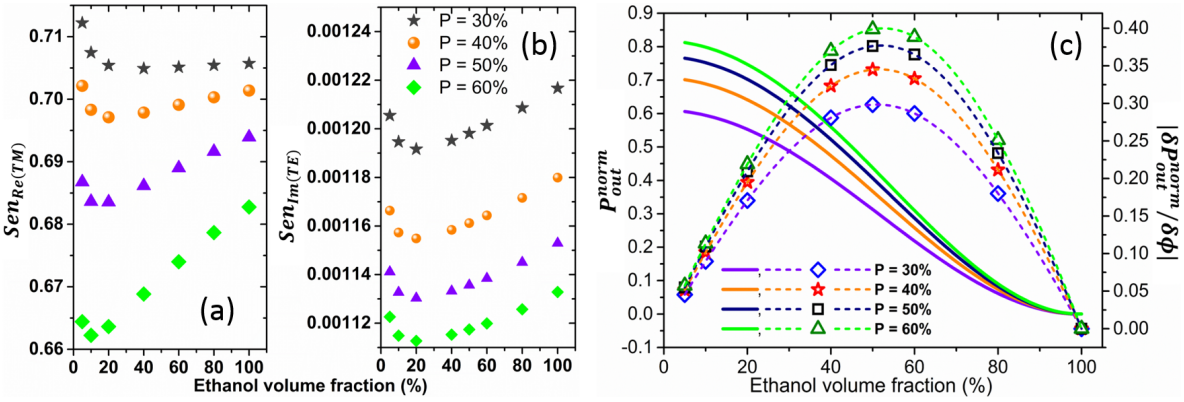

Figure 6. (a) and (b) indicate the CPWG quasi-TM real effective index sensitivity ($Sen_{Re(TM)}$) and normalized attenuation sensitivity ($Sen_{Im(TM)}$) variations with the ethanol volume fraction into horizontal slotted P-ZnO layer, respectively. (c) shows the variations of the normalized output power (P_{out}^{norm}) and the phase sensitivity ($|\delta P_{out}^{norm}/\delta\phi|$) shown by the solid and dashed lines, respectively.

The star, ball, triangle and diamond markers in Fig. 6(a) and (b) show the real effective index refractometric sensitivity ($Sen_Re(TM) = n_{eff}/n_{slot}$) and normalized mode attenuation sensitivity ($Sen_{Im(TM)} = k_{eff}/n_{slot}$) of the fundamental quasi-TM mode for P-ZnO layer having porosity, P = 30%, 40%, 50% and 60%, respectively.

For each P-ZnO layer, the $Sen_Re(TM)$ and $Sen_Im(TM)$ initially decrease up to 15% ethanol absorption and then increases with the ethanol volume fraction. Fig. 6(a) and (b) also indicate that a P-ZnO layer with lower porosity (P = 30%) shows higher $Sen_Re(TM)$ and $Sen_Im(TM)$ (stars) than a P-ZnO layer with higher porosity (P = 60%), shown by the diamond markers. Thus,for the waveguide based sensor design, the $Sen_Re(TM)$ is more important than $Sen_Im(TM)$. Figure 6(a) shows a much higher sensitivity (0.71 per RIU) can be achieved with our proposed CPWG structure. Besides, Fig. 6(b) reveals that the normalized attenuation of the CPWG is less sensitive to slot refractometric changes. This indicates a very small loss change due to different volume fraction of ethanol into P-ZnO. Results show a P-ZnO layer with lower porosity shows higher effectiveness.

The effective index change during ethanol or methanol vapor sensing process could be determined by using a Mach-Zehnder interferometer (MZI) as a transducer device. In the MZI two parallel arms are connected with one input and one output by using well designed 3 dB optical splitter. Our proposed CPWG is incorporated in the MZI sensing arm that passes through the ethanol or methanol contained gas chamber while another CPWG is used in reference arm. The insertion phase difference ($\Delta\phi$) between sensing and reference arm could be measured from the effective index change (n_{eff}) due different volume fraction of ethanol, as

$$\Delta\phi = \frac{2\pi}{\lambda} n_{eff}.L \tag{4}$$

Here, the MZI arm length is denoted by L. A destructive interference occurs due to the π phase difference that results a zero MZI output. The MZI arm length are calculated as 7.51, 6.02, 5.15 and 4.59 μm for each type of P-ZnO layer having porosity, P = 30%, 40%, 50% and 60%, respectively. Thus, higher porosity gives higher n_{eff} which results shorter arm length L. The normalized output power (P_{out}^{norm}) of the plasmonic waveguide assisted MZI carries the (n_{eff}) information in terms of ϕ, is given by

$$P_{out}^{norm} = \frac{1}{2}\, e^{-(2\alpha+\Delta\alpha_{sen})L} cosh(\Delta\alpha_{sen}L)(1 + Vcos\Delta\phi) \tag{5}$$

Here, $\Delta\alpha_{sen}$ denotes the mode attenuation change due to small change in the volume fraction of the ethanol or methanol into P-ZnO layer. P_{out}^{norm} is only measurable parameter that changes with the phase difference in between sensing and reference arms. Thus, a phase sensitivity ($\delta P_{out}^{norm}/\delta\phi$) of the device is an essential parameter that can be defined as

$$\frac{\delta P_{out}^{norm}}{\delta\phi} = -\frac{1}{2}\, e^{-(2\alpha+\Delta\alpha_{sen})L} cosh(\Delta\alpha_{sen}L)Vsin\Delta\phi \tag{6}$$

Where, V denotes the visibility parameter of the MZI. Figure 6(c) shows the normalized output power (P_{out}^{norm}) and absolute value of phase sensitivity ($|\delta P_{out}^{norm}/\delta\phi|$) variations of proposed CPWG incorporated MZI against ethanol volume fraction for different P-ZnO. The equation shows that the maximum phase sensitivity occurs for $\Delta\phi = \pi/2$. Purple, orange, blue and green solid lines indicate cosine variations of P_{out}^{norm} with volume fraction of ethanol into P-ZnO of porosity, P = 30%, 40%, 50% and 60%, respectively. 100% ethanol vapor absorption in sensing arm produces a π phase difference which results in a zero MZI output and a 5% (minimum) volume fraction of ethanol or methanol imposes a minimum phase difference with maximum 60%, 70%, 76% and 81% light output for 30%, 40%, 50% and 60% Porosity, respectively. Blue diamond, red star, black square and green triangles with purple, orange, blue and green dashed lines depict a sinusoidal variation of ($|\delta P_{out}^{norm}/\delta\phi|$) for four different P-ZnO layers. Lower porosity (P = 30%) shows lower phase sensitivity whereas, the green dashed line with triangular marker shows a much better phase sensitivity for porosity, P = 60%. Considering device sensitivity, all ZnO layers with different porosity, P = 30%, 40%, 50% and 60% exhibit maximum phase sensitivities of 0.30, 0.34, 0.38 and 0.40 when 51.6%, 52.1%, 52.6% and 53.2% of the ZnO pores are filled by the condensed ethanol or methanol, respectively when an exact $\pi/2$ phase difference is obtained in between sensing and reference arms. A MZI with lossless identical waveguide exhibits almost same phase sensitivities for all P-ZnO layers. In the plasmonic assisted MZI the attenuation imbalance between reference and sensing arm may affect the MZI output visibility (V). In this study, all volume fractions of ethanol or methanol into 30%, 40%, 50% and 60% P-ZnO the fringe contrast or visibility (V) was 0.99. This indicates that the extra attenuation was very small to cause any noticeable effect in the CPWG incorporated MZI performance.

5. CONCLUSIONS

A SOI based composite plasmonic waveguide (CPWG) is investigated and a compact MZI is designed where a porous ZnO layer is used as a horizontal slot for ethanol or methanol vapor sensing. A **H**-field based full vectorial FEM is used for modal analyses. Simulation results revel that the CPWG can guide a hybrid plasmonic supermode over a sufficiently long distance. All the design parameters are optimized and the proposed CPWG shows a high waveguide sensitivity of 0.7 per RIU for 40% P-ZnO layer as horizontal slot. Based on the simulated results, our designed CPWG incorporated MZI shows potential application in the field of environmental monitoring and hazardous chemical vapor sensing.

ACKNOWLEDGMENTS

This work was supported in part by City, University of London, UK and by Erasmus Mundus AREAS+ Ph.D. fellowship and SPIE Optics and Photonics Education Scholarship 2017 program for PhD and research funding.

REFERENCES

[1] Ghosh, S. and Rahman, B. M. A., "Evolution of plasmonic modes in a metal nano-wire studied by a modified finite element method," *Journal of Lightwave Technology* **PP**(99), 1–1 (2017).

[2] Alam, M., Aitchsion, J. S., and Mojahedi, M., "Compact hybrid tm-pass polarizer for silicon-on-insulator platform," *Applied optics* **50**(15), 2294–2298 (2011).

[3] Lu, F., Li, T., Xu, J., Xie, Z., Li, L., Zhu, S., and Zhu, Y., "Surface plasmon polariton enhanced by optical parametric amplification in nonlinear hybrid waveguide," *Optics express* **19**(4), 2858–2865 (2011).

[4] Homola, J., Yee, S. S., and Gauglitz, G., "Surface plasmon resonance sensors," *Sensors and Actuators B: Chemical* **54**(1), 3–15 (1999).

[5] Berk, A., "Variational principles for electromagnetic resonators and waveguides," *IRE Transactions on Antennas and Propagation* **4**(2), 104–111 (1956).

[6] Rahman, B. and Davies, J., "Finite-element solution of integrated optical waveguides," *Journal of Lightwave Technology* **2**(5), 682–688 (1984).

[7] Rahman, B. A. and Davies, J. B., "Penalty function improvement of waveguide solution by finite elements," *IEEE Transactions on Microwave Theory and Techniques* **32**(8), 922–928 (1984).

[8] Garahan, A., Pilon, L., Yin, J., and Saxena, I., "Effective optical properties of absorbing nanoporous and nanocomposite thin films," *Journal of applied physics* **101**(1), 014320 (2007).